

Full-Pose Geometric Tracking Control on $SE(3)$ for Laterally Bounded Fully-Actuated Aerial Vehicles

Antonio Franchi¹, Ruggero Carli², Davide Bicego¹, and Markus Ryll¹

Abstract— We introduce a control strategy for fully-actuated aerial vehicles to independently track trajectories in position and orientation. The technique is suited for platforms endowed with non-coplanar or vectoring-thrust rotors that change the orientation of the total thrust w.r.t. the body frame, thus achieving a complete exploitation of the 6 DoFs of the rigid body in 3D space. We introduce a new class of abstract aerial systems named Laterally Bounded Fully-Actuated vehicles (LBFA), in which most of the control authority is expressed along a principal thrust direction, while in the lateral directions a typically weaker force can be exploited to achieve full-pose tracking. LBFA systems naturally generalize underactuated aerial vehicles. We propose a geometric control for LBFAs that, once limited the set of admissible exerted forces within reasonable constraints, naturally extends the geometric control on $SE(3)$ for underactuated aerial vehicles. The exponential tracking of a feasible full-pose reference trajectory is proven using a Lyapunov technique in $SE(3)$. The controller can deal with both the *under-* and the *fully-actuated* configuration, without any issue of discontinuity. The controller guarantees the tracking of at least the positional part in the case that an unfeasible full-pose reference trajectory is provided.

I. INTRODUCTION

The amount of applications for autonomous aerial vehicles (i.e., Unmanned Aerial Vehicles (UAVs), Micro Aerial Vehicles (MAVs), etc.) has been heavily increasing throughout the last years, and nowadays these robotic/autonomous platforms are quickly becoming a mature technology, thanks to their versatility in performing a wide variety of different tasks. Small UAVs can replace human intervention in dangerous environments involving tough and uneasy operations, such as exploration, search and rescue, and scientific data gathering [1], [2], [3]. Other employments of these vehicles range from wide-angle aerial photography to inspection, surveillance and mapping of areas. Nevertheless, UAVs have been broadly used in many academic circles and research projects [4], [5], [6], to test algorithms and develop new sophisticated control strategies. Finally, a new field of complex tasks is represented by the physical interaction with the surrounding environment, i.e., single and multi-robot grasping and manipulation [7], [8]. All these instances underline the importance and the usefulness of studying this topic, while giving a strong motivation for the achievement of further improvements.

¹LAAS-CNRS, Université de Toulouse, CNRS, Toulouse, France, afranchi@laas.fr, dbicego@laas.fr, mryll@laas.fr

²Department of Information Engineering, University of Padova, Padova, Italy, carlirug@dei.unipd.it

This work has been partially funded by the European Union's Horizon 2020 research and innovation programme under grant agreement No 644271 AEROARMS

A standard quadrotor, like other common aerial platforms, is an under-actuated mechanical system, since it has to cope with the 6 degrees of freedom (DoFs) (3 translational DoFs and 3 rotational DoFs), owning only 4 control inputs. Presence of such an underactuation does not only limit the set of maneuvers that the UAV can carry out, but even deteriorates its potentiality to interact with the environment by exerting forces in an arbitrarily-chosen direction of the space. The main disadvantage of standard, *underactuated* UAVs, in our eyes, is the application of the control force, namely the total thrust, only in one pre-assigned direction in body frame, being usually the one perpendicular to the propeller rotation plane. This could be a serious problem in case the platform should move through a hostile and cluttered ambient or resist a wind gust while keeping a desired attitude, to mention some instances. For this reason, new actuation strategies that can overcome the aforementioned issue and then allow a complete tracking in position and attitude have been explored.

One circumvention to this drawback is mounting motors in a tilted way such that the thrust of each propeller is not collinear anymore. Results achieved in [9] and in [10] shows an improvement in resisting an opposing wrench. Furthermore, the work done in [11] and in [12] shows that once the system gains fully actuation, it is able to decouple the tracking of a desired position and orientation.

In this paper we propose a novel *geometric control* in $SE(3)$ that extends the work done in [13] to the case of Fully-Actuated Aerial Vehicles, such as, e.g., the one described in [9], [10], [12]. Furthermore we formally prove the asymptotically exponential tracking capabilities of the novel geometric control. The extension is clearly non-trivial, since the controller in [13] was specifically developed for an underactuated quadrotor system in order to track a 4D pose, i.e., the position in \mathbb{R}^3 plus only one orientation angle (typically the yaw). Instead here we generalize the geometric approach to any non-coplanar multirotor system to track a full 6D pose in $SE(3)$, and we also take into account the actuation limits along the lateral directions.

We first define the class of *laterally bounded fully-actuated (LBFA) aerial vehicle* in which a meaningful constraint for the total force that the platform can exert is introduced. Then the proposed controller ensures, if possible, the tracking of a full 6D pose reference trajectory. If the reference orientation and the force needed to track the position trajectory do not comply with the constraints, then the strategy adopted is to give priority to the tracking of the desired position while also tracking the closest feasible orientation to the reference one. This choice is supported by, e.g., the fact that in typical

applications a wrong position tracking is more likely to lead to an obstacle crash than a wrong orientation tracking.

The proposed controller is suitable for a large variety of different real platforms, and works seamlessly from the under- to the fully-actuated case, and vice-versa. For example in the case that the aerial vehicle loses its ability to exert a lateral force, than the proposed controller automatically and smoothly degenerates to the controller in [13].

The remaining part of the Paper is structured as follows. In Sec. II we first thoroughly discuss the usefulness of LBFA-aerial vehicles and then present their generic model. Then we present the full-pose geometric control and prove of the asymptotically exponential tracking in Sec. III. In Sec. IV we present the full computation of the generic controller in a meaningful case, while results of different simulations are shown in Sec. V. Finally we conclude the paper and give an outline of further possible extensions in Sec. VI.

II. LATERALLY BOUNDED FULLY-ACTUATED VEHICLES

In this section we provide first a motivation and state of the art regarding the LBFA class of vehicles (in Sec. II-A) and then we formally introduce the corresponding dynamic model and constraints (in Sec. II-B).

A. Motivations and State of the Art

In order to use at best the available energy, common multi-rotor platforms are designed with all coplanar rotors. Therefore the direction of the input force applied to the platform center of mass (the total thrust) is also collinear with the spinning axes of the rotors. Being the direction of the total thrust constant in body frame, those platforms are underactuated. For these platforms several controllers have been proposed in the literature like, e.g., controller based on the dynamic feedback linearization [14], cascaded/backstepping controllers [15], and geometric controllers on $SE(3)$ [13], just to mention a few.

In the recent years new platforms have been developed where the use of non-coplanar propellers [9], [11], [12], [16] allows the orientation of the total thrust to deviate from its principal direction, if needed. However, in order to minimize the waste of energy caused by the appearance of internal forces, the amount of total thrust in the lateral direction is typically kept significantly bounded.

Driven by the interest for those new kind of aerial platforms, we here develop a controller for laterally bounded fully-actuated aerial vehicle models which is a generalization of the classical underactuated multi-rotor. An LBFA possesses a *principal* direction of thrust along which most of the thrust can be exerted. A certain amount of thrust (typically smaller) can be exerted along any non-principal (lateral) directions. This model reduces to a standard underactuated multi-rotor vehicle when no thrust is possible along the non-principal direction, and to the (laterally unbounded) fully actuated platform when any amount of total thrust in the lateral directions is feasible.

An underactuated platform is not able to track a full-pose trajectory, i.e., a trajectory with independent position and orientation in $SE(3)$. In fact, the rotations about any axis that is orthogonal to the body-frame fixed total thrust direction,

TABLE I
MAIN SYMBOLS USED IN THE PAPER

Definition	Symbol
World Inertial Frame	\mathcal{F}_W
Attached Body Frame	\mathcal{F}_B
Position of the O_B , the CoM, in \mathcal{F}_W	\mathbf{p}
Rotation matrix from \mathcal{F}_B to \mathcal{F}_W	\mathbf{R}
Angular velocity of \mathcal{F}_B w.r.t \mathcal{F}_W expr. in \mathcal{F}_B	$\boldsymbol{\omega}$
Mass of the vehicle	m
Vehicle's Inertia matrix w.r.t to O_B expressed in \mathcal{F}_B	\mathbf{J}
Control force applied to the CoM expressed in \mathcal{F}_B	\mathbf{u}_1
Control moment applied to the CoM expressed in \mathcal{F}_B	\mathbf{u}_2
Feasible set of the control force \mathbf{u}_1	\mathcal{U}_1
Feasible set of the projection of \mathbf{u}_1 on the xy plane in \mathcal{F}_B	\mathcal{U}_{xy}
Reference position for O_B in \mathcal{F}_W	$\mathbf{p}_r(t)$
Reference rotation matrix from \mathcal{F}_B to \mathcal{F}_W	$\mathbf{R}_r(t)$
Reference control force to be applied to O_B	$\mathbf{f}_r(t)$
Set of orientations in $SO(3)$ that allow the application of $\mathbf{f}_r(t)$	$\mathcal{R}(\mathbf{f}_r)$
Subset of $\mathcal{R}(\mathbf{f}_r)$ that minimizes a certain cost w.r.t. \mathbf{R}_r	$\overline{\mathcal{R}}(\mathbf{f}_r, \mathbf{R}_r)$
Desired rotation matrix in $\overline{\mathcal{R}}(\mathbf{f}_r, \mathbf{R}_r)$	\mathbf{R}_d

must follow the evolution over time of the position trajectory, due to the well-known differential flatness property [14], [17]. The rotation about the axis that is parallel to the total thrust is instead independent from the position trajectory. We summarize this fact saying that an underactuated multi-rotor aerial platform can only track a 4D-pose trajectory (i.e., position plus one angle).

If instead some force can be exerted in the lateral direction, like in the case of a generic LBFA vehicles, the platform is fully actuated and capable of tracking a full-pose 6D trajectory (position plus three angles). However due to the bounded thrust along the lateral directions, it is not possible to track *any* full-pose trajectory. The larger the bounds the higher the ability of the platform to track any trajectory, the lower the bounds the more the platform resembles an underactuated multi-rotor and thus becomes almost unable to track a full-pose 6D trajectory but only a 4D-pose one.

In the literature a few other control schemes for fully actuated aerial vehicles have been proposed. Both approaches presented in [11], [12] are works on a particular fully actuated, namely a hexarotor and a quadrotor. Both controllers are based on (dynamic) feedback linearization. In [18] a controller that deals with fully-actuated platforms is presented, which is specific to vectoring thrust (tiltable-propeller) aerial vehicles, thus not the same as the LBFA aerial vehicles considered here. Finally in [16] the design and the control of a fully actuated octorotor platform is presented, which is however specific to that platform, it does not consider the lateral bounds, and it is based on a particular Euler angle representation.

In this paper we present a geometric controller that is a nontrivial extension of the 4D-pose trajectory controller for underactuated vehicles [13] to full-pose 6D trajectory tracking for LBFA aerial vehicles. Our approach is very general and applicable to any LBFA vehicle, thus also taking into account the bounds on the lateral control force. The method is not prone to local orientation representation singularities since it is natively designed in $SE(3)$. Furthermore, being not based on pure model inversion like feedback linearization, it is structurally more robust to model uncertainties.

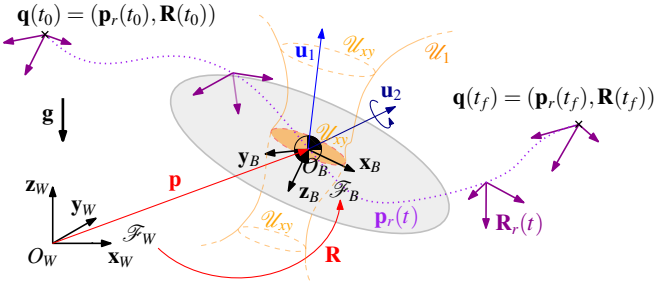


Fig. 1. A drawing illustrating the main the quantities of a LBFA Aerial Vehicle, the main frames involved, the laterally bounded input sets, and the full-pose 6D reference trajectory.

B. Dynamic Model

With reference to Fig. 1, we denote with $\mathcal{F}_W = O_W, \{\mathbf{x}_W, \mathbf{y}_W, \mathbf{z}_W\}$ and $\mathcal{F}_B = O_B, \{\mathbf{x}_B, \mathbf{y}_B, \mathbf{z}_B\}$ the fixed inertial frame, and body frame attached to the aerial platform, respectively. The origin of \mathcal{F}_B , i.e., O_B , is chosen coincident with the center of mass (CoM) of the platform and its position in \mathcal{F}_W is denoted with $\mathbf{p}_{O_B}^W \in \mathbb{R}^3$, shortly indicated with just \mathbf{p} in the following. For the reader convenience, Table I summarizes all the main symbols used in the paper.

The aerial platform is modeled as a rigid body whose mass is denoted with $m > 0$. The positive definite matrix $\mathbf{J} \in \mathbb{R}^{3 \times 3}$ denotes the vehicle inertia matrix with respect to O_B expressed in \mathcal{F}_B . The orientation of \mathcal{F}_B with respect to \mathcal{F}_W is represented by the rotation matrix $\mathbf{R}_B^W \in SE(3)$, shortly denoted with \mathbf{R} in the following. The configuration of the aerial vehicle is defined by the position \mathbf{p} and the attitude \mathbf{R} , which are gathered in the vehicle configuration $\mathbf{q} = (\mathbf{p}, \mathbf{R}) \in SE(3)$.

The angular velocity of \mathcal{F}_B with respect to \mathcal{F}_W , expressed in \mathcal{F}_B , is indicated with $\boldsymbol{\omega}_{B,F}^B \in \mathbb{R}^3$, and briefly denoted as $\boldsymbol{\omega}$ in the following. Thus, the vehicle orientation kinematics is described by:

$$\dot{\mathbf{R}} = \mathbf{R}[\boldsymbol{\omega}]_{\times}, \quad (1)$$

where $[\star]_{\times} : \mathbb{R}^3 \rightarrow so(3)$ is the map that associates a vector $\star \in \mathbb{R}^3$ to its corresponding skew symmetric matrix.

Let us denote the control inputs of the vehicle with $\mathbf{u}_1 = [u_1 \ u_2 \ u_3]^T \in \mathbb{R}^3$ and $\mathbf{u}_2 = [u_4 \ u_5 \ u_6]^T \in \mathbb{R}^3$, representing the total force and total moment applied to the CoM of the vehicle expressed in \mathcal{F}_B , respectively. The total force input \mathbf{u}_1 is subject to the following constraints

$$[u_1 \ u_2]^T \in \mathcal{U}_{xy} \subset \mathbb{R}^2, \quad (2)$$

$$u_3 \geq 0, \quad (3)$$

where the *laterally bounding* set \mathcal{U}_{xy} is a set that contains the origin. We define $\mathcal{U}_1 = \{\mathbf{u}_1 \in \mathbb{R}^3 \mid [u_1 \ u_2]^T \in \mathcal{U}_{xy}, u_3 \geq 0\}$. Note that \mathcal{U}_{xy} can be constant or even be changing depending of u_3 , as shown in Figures 1 and 2–(left).

Using the Newton-Euler approach we can express the dynamics of the aerial platform as

$$m\ddot{\mathbf{p}} = -m\mathbf{g}\mathbf{e}_3 + \mathbf{R}\mathbf{u}_1 \quad (4)$$

$$\mathbf{J}\dot{\boldsymbol{\omega}} = -\boldsymbol{\omega} \times \mathbf{J}\boldsymbol{\omega} + \mathbf{u}_2 \quad (5)$$

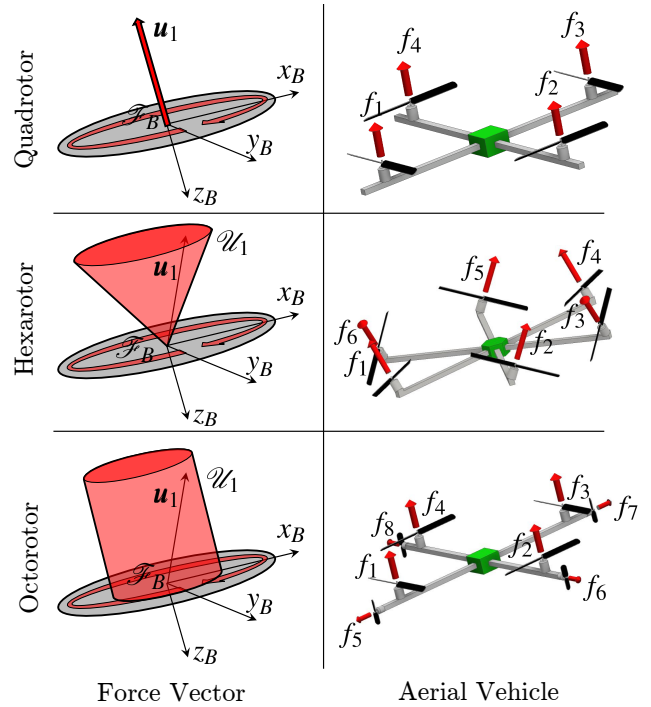


Fig. 2. Set of allowable total total thrust \mathcal{U}_1 for 3 basic different cases of LBFA platforms. Top: a standard quadrotor. Middle: an hexarotor with tilted propellers or vectored thrust coaxial rotor. Bottom: an octorotor with smaller lateral propellers. In the last two cases the set are an approximation of the real cases, which can be used to simplify the computations. However the proposed control can deal with the real more complex sets as well.

with g being the gravitational acceleration and \mathbf{e}_i , $i = 1, 2, 3$, representing the i -th vector of the canonical basis of \mathbb{R}^3 .

Remark II.1 (Underactuated aerial vehicle). When

$$\mathcal{U}_{xy} = \{\mathbf{0}\} \quad (6)$$

the total force is always oriented as \mathbf{Re}_3 and model (4)–(5) becomes the underactuated quadrotor model considered in [13]–[15], see Fig. 2–(top).

Remark II.2 (Conic LBFA). When

$$\mathcal{U}_{xy} = \{[u_1 \ u_2]^T \in \mathbb{R}^2 \mid u_1^2 + u_2^2 \leq (\tan \alpha)^2 u_3^2\}, \quad (7)$$

model (4)–(5) approximates the case of hexarotors with tilted propellers [9], [12], and of vectored thrust coaxial rotor vehicles [19], for which the set of allowable \mathcal{U}_1 forces has the conic shape depicted in Fig. 2–(middle). The quantity α is a parameter that represents the tilting angle of the propellers (hexarotor) or the maximum tilting angle (vectored thrust coaxial rotor vehicle).

Remark II.3 (Cylindric LBFA). When

$$\mathcal{U}_{xy} = \{[u_1 \ u_2]^T \in \mathbb{R}^2 \mid u_1^2 + u_2^2 \leq r_{xy}^2\}, \quad (8)$$

model (4)–(5) approximates the case of an octorotor (or, more in general, an n -rotor) with four main propellers and four (or $n - 4$) secondary less powerful propellers tilted 90 degrees w.r.t. the main ones, like the one presented in [16], for which the set of allowable \mathcal{U}_1 forces can be approximated

by the cylindrical shape depicted in Fig. 2-(bottom). Note that a more accurate (e.g., parallelepipedal) set can be used if needed, for which the proposed controller is still valid. The constant parameter r_{xy} represents the maximum lateral thrust allowed by the smaller horizontal propellers.

III. FULL-POSE GEOMETRIC CONTROL ON SE(3)

Let be given a full-pose trajectory $\mathbf{q}_r(t) = (\mathbf{p}_r(t), \mathbf{R}_r(t)) : [t_0, t_f] \rightarrow SE(3)$, where $\mathbf{p}_r(t) \in \mathbb{R}^3$ is the reference position trajectory and $\mathbf{R}_r(t) \in SO(3)$ is the reference attitude trajectory. The nominal input required to track $\mathbf{q}_r(t)$ is easily obtained inverting (4)-(5)

$$\mathbf{u}_1^r = \mathbf{R}_r^T (m\mathbf{g}\mathbf{e}_3 + m\dot{\mathbf{p}}_r) \quad (9)$$

$$\mathbf{u}_2^r = \boldsymbol{\omega}_r \times \mathbf{J}\boldsymbol{\omega}_r + \mathbf{J}\dot{\boldsymbol{\omega}}_r, \quad (10)$$

where $\ddot{\mathbf{p}}_r = \frac{d^2}{dt^2}\mathbf{p}_r$, and $\boldsymbol{\omega}_r$ is defined using (1), i.e., $[\boldsymbol{\omega}_r]_\times = \mathbf{R}_r^T \dot{\mathbf{R}}_r$.

Definition 1. A reference trajectory $\mathbf{q}_r(t)$ is *feasible* if $\mathbf{u}_1^r(t) \in \mathcal{U}_1 \forall t \in [t_0, t_f]$.

Full-pose 6D tracking is possible only if the given reference trajectory $\mathbf{q}_r(t)$ is feasible. However our controller works even if $\mathbf{q}_r(t)$ is not feasible, in the sense that the tracking of $\mathbf{p}_r(t)$ is still guaranteed and no singularity appears. Consider the following position and velocity errors

$$\mathbf{e}_p = \mathbf{p} - \mathbf{p}_r \quad (11)$$

$$\mathbf{e}_v = \dot{\mathbf{p}} - \dot{\mathbf{p}}_r, \quad (12)$$

and the following vector

$$\mathbf{f}_r = m\ddot{\mathbf{p}}_r + m\mathbf{g}\mathbf{e}_3 - \mathbf{K}_p\mathbf{e}_p - \mathbf{K}_v\mathbf{e}_v, \quad (13)$$

where \mathbf{K}_p and \mathbf{K}_v are positive definite gain matrices. The vector \mathbf{f}_r represents the reference total control force that ideally one would like to apply to the aerial vehicle CoM if the system would be completely fully actuated, i.e., if $\mathcal{U}_1 = \mathbb{R}^3$.

The set of orientations that allow to apply \mathbf{f}_r to the CoM of the LBFA aerial vehicle is defined as

$$\mathcal{R}(\mathbf{f}_r) = \{\mathbf{R} \in SO(3) \mid \mathbf{R}^T \mathbf{f}_r \in \mathcal{U}_1\}. \quad (14)$$

For an underactuated coplanar multi-rotor system, i.e., if (6) holds, the set $\mathcal{R}(\mathbf{f}_r)$ is formed by any \mathbf{R} such that $\mathbf{R}\mathbf{e}_3$ and \mathbf{f}_r are parallel, i.e., $\mathbf{R}\mathbf{e}_3 \times \mathbf{f}_r = \mathbf{0}$. For a generic LBFA aerial vehicle the set $\mathcal{R}(\mathbf{f}_r)$ may contain also matrixes for which $\mathbf{R}\mathbf{e}_3 \times \mathbf{f}_r \neq \mathbf{0}$. Therefore we have the following.

Proposition 1. For any \mathbf{f}_r it holds $\mathcal{R}(\mathbf{f}_r) \neq \emptyset$.

Proof. If $\mathbf{f}_r \neq \mathbf{0}$ then, by definition of $\mathcal{R}(\mathbf{f}_r)$ and \mathcal{U}_1 ,

$$\mathcal{R}(\mathbf{f}_r) \supset \left\{ \mathbf{R} \in SO(3) \mid \mathbf{R}\mathbf{e}_3 = \frac{\mathbf{f}_r}{\|\mathbf{f}_r\|} \right\} \neq \emptyset$$

If $\mathbf{f}_r = \mathbf{0}$ then $\mathcal{R}(\mathbf{f}_r) = SO(3)$. \square

As one can see from the LBFA model the rotational dynamics (5) is (completely) fully actuated and decoupled from the translational dynamics (4). One of the main ideas behind the proposed controller is to exploit this cascaded structure by choosing, at each time t , a desired orientation

$\mathbf{R}_d \in SO(3)$ that belongs to $\mathcal{R}(\mathbf{f}_r)$ and also minimizes a given cost function w.r.t. \mathbf{R}_r . Then one can use the fully actuated rotational dynamics to track \mathbf{R}_d and, in turns, track the reference position \mathbf{p}_r . If the full-pose reference trajectory \mathbf{q}_r is feasible then \mathbf{R}_d will exponentially converge to \mathbf{R}_r and then also the reference orientation will be tracked. Otherwise, only the best feasible orientation will be tracked. Therefore the controller implicitly prioritizes the position trajectory against the orientation one, as wanted. In the following, we shall formally define this controller concept and theoretically prove its convergence properties.

Define $\overline{\mathcal{R}}(\mathbf{f}_r, \mathbf{R}_r) \subset \mathcal{R}(\mathbf{f}_r)$ as the set of rotation matrices that solve the minimization

$$\min_{\mathbf{R}' \in \overline{\mathcal{R}}(\mathbf{f}_r)} J(\mathbf{R}_r, \mathbf{R}'), \quad (15)$$

where $J : SO(3) \times SO(3) \rightarrow \mathbb{R}_{\geq 0}$ is a suitably chosen cost function that may represent, e.g., the degree of similarity between \mathbf{R}_r and \mathbf{R}' one is interested in. The elements in $\overline{\mathcal{R}}(\mathbf{f}_r, \mathbf{R}_r)$ represent orientations of the LBFA that allow to apply \mathbf{f}_r and minimize the function J w.r.t. \mathbf{R}_r .

Consider that, at each time t a desired orientation $\mathbf{R}_d \in \overline{\mathcal{R}}(\mathbf{f}_r, \mathbf{R}_r)$ is chosen. Furthermore, whenever $\mathbf{R}_r \in \overline{\mathcal{R}}(\mathbf{f}_r, \mathbf{R}_r)$ then \mathbf{R}_d must be chosen equal to \mathbf{R}_r .

Then define, as in [13], the rotation and angular velocity errors

$$\mathbf{e}_R = \frac{1}{2}(\mathbf{R}_d^T \mathbf{R} - \mathbf{R}^T \mathbf{R}_d)^\vee, \quad (16)$$

$$\mathbf{e}_\omega = \boldsymbol{\omega} - \mathbf{R}\mathbf{R}_d^T \boldsymbol{\omega}_d \quad (17)$$

where $\bullet^\vee : so(3) \rightarrow \mathbb{R}^3$ is the inverse map of $[\star]_\times$, and $\boldsymbol{\omega}_d$ is the angular velocity associated to \mathbf{R}_d .

Consider then the following control law

$$\mathbf{u}_1 = \text{sat}_{\mathcal{U}_{xy}}((\mathbf{f}_r^T \mathbf{R}\mathbf{e}_1)\mathbf{e}_1 + (\mathbf{f}_r^T \mathbf{R}\mathbf{e}_2)\mathbf{e}_2) + \max\{0, (\mathbf{f}_r^T \mathbf{R}\mathbf{e}_3)\}\mathbf{e}_3 \quad (18)$$

$$\mathbf{u}_2 = \boldsymbol{\omega} \times \mathbf{J}\boldsymbol{\omega} - \mathbf{K}_R \mathbf{e}_R - \mathbf{K}_\omega \mathbf{e}_\omega + \mathbf{J}([\boldsymbol{\omega}]_\times \mathbf{R}^T \mathbf{R}_d \boldsymbol{\omega}_d - \mathbf{R}^T \mathbf{R}_d \dot{\boldsymbol{\omega}}_d) \quad (19)$$

where $\text{sat}_{\mathcal{U}_{xy}}(\mathbf{x})$ is a vector in \mathcal{U}_{xy} with the same direction of \mathbf{x} , that minimizes the distance from \mathbf{x} . $\mathbf{K}_R = k_R \mathbf{I}$ and $\mathbf{K}_\omega = k_\omega \mathbf{I}$ are two scalar gain matrices with $k_R > 0$ and $k_\omega > 0$.

Note that (18)–(19) reduces to the control in [13] in the case that (6) holds. However a major difference is in the computation of \mathbf{R}_d , which in [13] is computed from the position trajectory using the differential flatness property while in the proposed controller is computed ensuring feasibility of the input and minimizing the cost function w.r.t. the reference orientation \mathbf{R}_r .

In order to prove the convergence properties of the proposed controller let us consider, as in [13], the following error function between two rotation matrixes \mathbf{R}_1 and \mathbf{R}_2 to be

$$d(\mathbf{R}_1, \mathbf{R}_2) = \frac{1}{2} \text{tr}(\mathbf{I} - \mathbf{R}_2^T \mathbf{R}_1). \quad (20)$$

Theorem 1. Assume that $\mathbf{R}_d(t) \in \overline{\mathcal{R}}(\mathbf{f}_r(t))$ for any t and that $\boldsymbol{\omega}_d(t)$ and $\dot{\boldsymbol{\omega}}_d(t)$ are well defined for any t . Consider the control \mathbf{u}_1 and \mathbf{u}_2 defined at (18) and (19).

Assume that the initial condition satisfies

$$d(\mathbf{R}(0), \mathbf{R}_d(0)) < 2, \quad (21)$$

and

$$\|\mathbf{e}_\omega(0)\|^2 < \frac{2}{\lambda_{\min}(J)} k_R (1 - d(\mathbf{R}(0), \mathbf{R}_d(0))) \quad (22)$$

Then the tracking errors \mathbf{e}_R , \mathbf{e}_ω , \mathbf{e}_p and \mathbf{e}_v goes exponentially to zero.

Proof. The proof is divided into two parts. We first show that, if the $\mathbf{R}(0)$ and $\mathbf{e}_\omega(0)$ satisfy, respectively, (21) and (22), then $\mathbf{R}(t)$ converges exponentially to $\mathbf{R}_d(t)$, in the sense that the function $d(\mathbf{R}(t), \mathbf{R}_d(t))$ goes exponentially to zero. Secondly, we characterize the error dynamics on the translational dynamics and, based on the fact that $\mathbf{R}(t)$ converges exponentially to $\mathbf{R}_d(t)$ we show that also \mathbf{e}_p and \mathbf{e}_v goes exponentially to zero.

Consider (17). Then the time derivative of \mathbf{e}_ω is

$$\mathbf{J}\dot{\mathbf{e}}_\omega = \mathbf{J}\dot{\boldsymbol{\omega}} + \mathbf{J}([\boldsymbol{\omega}]_\times \mathbf{R}^T \mathbf{R}_d \boldsymbol{\omega}_d - \mathbf{R}^T \mathbf{R}_d \dot{\boldsymbol{\omega}}_d).$$

Plugging into the above equation the equation of motion (5) where \mathbf{u}_2 is given as in (19), we get

$$\mathbf{J}\dot{\mathbf{e}}_\omega = -k_R \mathbf{e}_R - k_\omega \mathbf{e}_\omega.$$

In [13], it is shown, by exhibiting a suitable Lyapunov function, that, under conditions in (21) and in (22), the zero equilibrium of the attitude tracking error \mathbf{e}_R , \mathbf{e}_ω is exponentially stable and that there exist two positive constants α, β such that

$$d(\mathbf{R}(t), \mathbf{R}_d(t)) < \alpha e^{-\beta t}. \quad (23)$$

We determine now the error dynamics of the translational dynamics. From (4) we can write

$$\begin{aligned} m\ddot{\mathbf{p}} &= -mg\mathbf{e}_3 + \mathbf{f}_r + \mathbf{R}\mathbf{u}_1 - \mathbf{f}_r \\ &= m\ddot{\mathbf{p}}_r - \mathbf{K}_p \mathbf{e}_p - \mathbf{K}_v \mathbf{e}_v + \boldsymbol{\gamma}, \end{aligned}$$

where $\boldsymbol{\gamma} = \mathbf{R}\mathbf{u}_1 - \mathbf{f}_r$. It easily follows that

$$m\dot{\mathbf{e}}_v = -\mathbf{K}_p \mathbf{e}_p - \mathbf{K}_v \mathbf{e}_v + \boldsymbol{\gamma}. \quad (24)$$

Since \mathbf{R} tends exponentially to \mathbf{R}_d and since $\mathbf{R}_d \in \mathcal{R}(\mathbf{f}_r)$ for any t , we have that \mathbf{u}_1 tends exponentially to $\mathbf{R}^T \mathbf{f}_r$. This implies that there exist two positive constants C, ρ such that

$$\|\boldsymbol{\gamma}(t)\| \leq C e^{-\rho t}.$$

Let $\mathbf{x} = [\mathbf{e}_v \ \mathbf{e}_p]^T$ then, (24) can be written in vector form as

$$\dot{\mathbf{x}} = \mathbf{A}\mathbf{x} + \mathbf{B}\boldsymbol{\gamma}$$

where

$$\mathbf{A} = \begin{bmatrix} -\mathbf{K}_v & -\mathbf{K}_p \\ \mathbf{I} & \mathbf{0} \end{bmatrix}, \quad \mathbf{B} = \begin{bmatrix} \mathbf{I} \\ \mathbf{0} \end{bmatrix}.$$

Since $\mathbf{K}_v, \mathbf{K}_p$ are both positive definite matrices, we have that \mathbf{A} is a stable matrix. From standard system theory, we get that

$$\mathbf{x}(t) = e^{\mathbf{A}(t-t_0)} \mathbf{x}(t_0) + \int_{t_0}^t e^{\mathbf{A}(t-\tau)} \mathbf{B}\boldsymbol{\gamma}(\tau) d\tau.$$

From the fact that \mathbf{A} is stable it follows that the term $e^{\mathbf{A}(t-t_0)} \mathbf{x}(t_0)$ goes exponentially to zero. The term

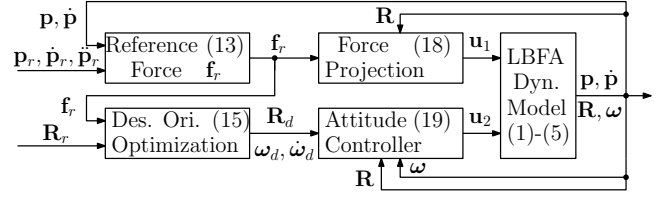


Fig. 3. Block diagram of the proposed geometric controller with the references to the corresponding equations in the text.

$\int_{t_0}^t e^{\mathbf{A}(t-\tau)} \mathbf{B}\boldsymbol{\gamma}(\tau) d\tau$ can be rewritten as the convolution between \mathbf{K} and $\boldsymbol{\gamma}$, i.e., $\int_{t_0}^t e^{\mathbf{A}(t-\tau)} \mathbf{B}\boldsymbol{\gamma}(\tau) d\tau = (\mathbf{K} * \boldsymbol{\gamma})(t)$ where

$$\mathbf{K}(t) = \begin{cases} e^{\mathbf{A}(t-t_0)} \mathbf{B} & \text{if } t \geq t_0 \\ \mathbf{0} & \text{if } t < t_0 \end{cases}$$

Since both \mathbf{K} and $\boldsymbol{\gamma}$ are exponentially decaying, we have that also $(\mathbf{K} * \boldsymbol{\gamma})(t)$ goes exponentially to zero. This concludes the proof. \square

A block diagram that shows the main subsystems of the proposed control architecture is provided in Fig. 3, where the reference to the corresponding equation is also contained in each block.

Theorem 1 ensures, under mild conditions, the exponential convergence to zero of \mathbf{e}_p , \mathbf{e}_v , \mathbf{e}_R , and \mathbf{e}_ω . Notice that this result holds regardless of the feasibility of \mathbf{q}_r . If \mathbf{q}_r is also feasible then exponential tracking of \mathbf{q}_r by \mathbf{q} is also guaranteed. In order to formally state this fact let us define the following errors

$$\mathbf{e}_R = \frac{1}{2} (\mathbf{R}_r^T \mathbf{R}_d - \mathbf{R}_d^T \mathbf{R}_r)^\vee, \quad (25)$$

$$\mathbf{e}_{\omega_r} = \boldsymbol{\omega}_d - \mathbf{R}_d \mathbf{R}_r^T \boldsymbol{\omega}_r \quad (26)$$

In the next result we characterize the convergence of the above errors to zero provided that the reference trajectory $\mathbf{q}_r(t)$ is *feasible* and satisfies the additional property that \mathbf{u}_1^r is *sufficiently inside* \mathcal{U}_1 , meaning that there exists a time instant \bar{t} and a positive number ε such that the distance of \mathbf{u}_1^r from the boundary of \mathcal{U}_1 is greater than ε for all $t > \bar{t}$, i.e.,

$$\text{dist}(\mathbf{u}_1^r(t), \partial\mathcal{U}_1) > \varepsilon, \quad \forall t > \bar{t}. \quad (27)$$

Theorem 2. Assume $\mathbf{q}_r(t)$ is a feasible trajectory and that it satisfies the additional property in (27). Assume that $\mathbf{R}_d(t) \in \mathcal{R}(\mathbf{f}_r(t))$ for any t and that $\boldsymbol{\omega}_d(t)$ and $\dot{\boldsymbol{\omega}}_d(t)$ are well defined for any t . Consider the control \mathbf{u}_1 and \mathbf{u}_2 defined at (18) and (19). Assume that the initial condition satisfies (21) and (22). Then the tracking errors \mathbf{e}_R , \mathbf{e}_ω , \mathbf{e}_p and \mathbf{e}_v goes exponentially to zero and there exists a time instant $\bar{t} \geq t_0$ such that $\mathbf{e}_{R_r}(t) = \mathbf{e}_{\omega_r}(t) = \mathbf{0}$ for all $t > \bar{t}$.

Proof. Observe that from the previous Theorem 1 we can write that

$$\mathbf{f}_r = m\ddot{\mathbf{p}}_r + mg\mathbf{e}_3 + \boldsymbol{\xi} \quad (28)$$

where

$$\|\boldsymbol{\xi}(t)\| \leq L e^{-\lambda t} \quad (29)$$

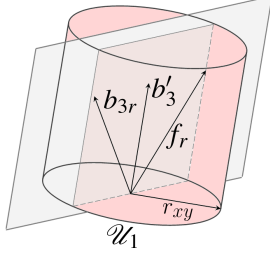


Fig. 4. geometrical interpretation of the feasibility constraint in (31).

for some positive constants L and λ . This implies that the vector $\mathbf{f}_r - (m\ddot{\mathbf{p}}_r + mg\mathbf{e}_3)$ and, in turn, also the vector $\mathbf{R}_r^T \mathbf{f}_r - \mathbf{R}_r^T (m\ddot{\mathbf{p}}_r + mg\mathbf{e}_3)$, tend exponentially to zero.

Hence, since $\mathbf{q}_r(t)$ is feasible and satisfies (27), it follows, from continuity arguments, that there exists t' such that $\mathbf{R}_r^T \mathbf{f}_r \in \mathcal{U}_1$ for all $t \geq t'$. Therefore $\mathbf{R}_d(t) = \mathbf{R}_r(t)$ for all $t > t'$. \square

IV. COMPUTATION OF \mathbf{R}_d FOR AN ILLUSTRATIVE CASE

The proposed control method is kept on purpose general regarding two main features: the choice of \mathcal{U}_{xy} in (2) and the choice of J in (15). The former allows the method to be used for a large set of aerial vehicles with different actuation capabilities. The latter allows the engineer to customize the definition of similarity between two orientations in order to comply with the particular task at hand. In this section we illustrate how these two general features are particularized to a specific meaningful case.

In particular, we consider the case of \mathcal{U}_{xy} defined in (8) and the following choice of cost function J

$$J(\mathbf{R}_r, \mathbf{R}') = 1 - \mathbf{b}_{3r}^T \mathbf{b}'_3, \quad (30)$$

where $\mathbf{R}_r = [\mathbf{b}_{1r} \mathbf{b}_{2r} \mathbf{b}_{3r}]$ and $\mathbf{R}' = [\mathbf{b}'_1 \mathbf{b}'_2 \mathbf{b}'_3]$. The cost function J in (30) is minimized whenever $\mathbf{b}_{3r} = \mathbf{b}'_3$ and maximized whenever $\mathbf{b}_{3r} = -\mathbf{b}'_3$.

Remark IV.1. For example in the case that the aerial vehicle embeds a down-facing camera, the cost (30) can be used to emphasize the fact that while following the position trajectory it is important to orient the sagittal axis of the camera as prescribed by \mathbf{b}_{3r} while the particular rotation about the sagittal axis has no relevance for the specific camera-observation task.

In the following we show how it is possible to efficiently compute an \mathbf{R}_d that belongs to $\mathcal{R}(\mathbf{f}_r, \mathbf{R}_r)$ and is also equal to \mathbf{R}_r if $\mathbf{R}_r \in \mathcal{R}(\mathbf{f}_r, \mathbf{R}_r)$. These are in fact the requirements needed for \mathbf{R}_d in order for Theorem 1 and Proposition 2 to be valid.

Let us start by instantiating $\mathcal{R}(\mathbf{f}_r)$ for this particular case. From simple geometrical considerations on the cylindrical shape of the set \mathcal{U}_1 it is easy to see that the following definition of $\mathcal{R}(\mathbf{f}_r)$ holds

$$\mathcal{R}(\mathbf{f}_r) = \left\{ \mathbf{R}' \in SO(3) \mid \mathbf{f}_r^T \mathbf{b}'_3 \geq \sqrt{\|\mathbf{f}_r\|^2 - r_{xy}^2} \right\}, \quad (31)$$

which states that the vector \mathbf{f}_r must lie within the cylinder of radius r_{xy} generated about the axis \mathbf{b}'_3 (see Fig. 4).

Algorithm 1: Bisection used to solve problem (33)

Data: n (number of iterations \propto solution accuracy)

Data: \mathbf{b}_{3r} , \mathbf{f}_r , and r_{xy} (givens of the problem)

```

1  $\mathbf{k} \leftarrow \frac{\mathbf{b}_{3r} \times \mathbf{f}_r}{\|\mathbf{b}_{3r} \times \mathbf{f}_r\|}$ 
2  $\theta_{max} \leftarrow \arcsin(\|\mathbf{k}\|)$ 
3  $\theta \leftarrow \theta_{max}/2$ 
4 for  $i = 1$  to  $n$  do
5   if  $\mathbf{f}_r^T \mathbf{b}'_{3\parallel}(\theta) \geq \sqrt{\|\mathbf{f}_r\|^2 - r_{xy}^2}$  then
6      $\theta \leftarrow \theta - \frac{1}{2} \frac{\theta_{max}}{2^i}$ 
7   else
8      $\theta \leftarrow \theta + \frac{1}{2} \frac{\theta_{max}}{2^i}$ 
9 return  $\theta$ 

```

Using (30) and (31) we can rewrite (15) in terms of the only vector variable \mathbf{b}'_3 , instead of the whole matrix \mathbf{R}' , as

$$\min_{\substack{\mathbf{f}_r^T \mathbf{b}'_3 \geq \sqrt{\|\mathbf{f}_r\|^2 - r_{xy}^2} \\ \|\mathbf{b}'_3\|^2 = 1}} -\mathbf{b}_{3r}^T \mathbf{b}'_3, \quad (32)$$

where r_{xy}^2 , \mathbf{f}_r^T and \mathbf{b}_{3r}^T are the givens of the problem.

In the case that $\mathbf{f}_r^T \mathbf{b}_{3r} \geq \sqrt{\|\mathbf{f}_r\|^2 - r_{xy}^2}$ then $\mathbf{b}'_3 = \mathbf{b}_{3r}$ is the solution to (32). Otherwise let us write \mathbf{b}'_3 as the sum of two components $\mathbf{b}'_3 = \mathbf{b}'_{3\parallel} + \mathbf{b}'_{3\perp}$, where $\mathbf{b}'_{3\parallel}$ is parallel to the plane spanned by \mathbf{b}_{3r} and \mathbf{f}_r and $\mathbf{b}'_{3\perp}$ is perpendicular to it, i.e., is parallel to $\mathbf{b}_{3r} \times \mathbf{f}_r$. It is easy to see that the cost function in (32), i.e., $\mathbf{b}_{3r}^T \mathbf{b}'_3$, is not affected by $\mathbf{b}'_{3\perp}$, in fact

$$\mathbf{b}_{3r}^T \mathbf{b}'_3 = \underbrace{\mathbf{b}_{3r}^T \mathbf{b}'_{3\perp}}_{=0} + \mathbf{b}_{3r}^T \mathbf{b}'_{3\parallel} = \mathbf{b}_{3r}^T \mathbf{b}'_{3\parallel}.$$

The vector $\mathbf{b}_{3\parallel}$ can be written using the Rodrigues' rotation formula as

$$\mathbf{b}'_{3\parallel}(\theta) = \mathbf{b}_{3r} \cos \theta + (\mathbf{k} \times \mathbf{b}_{3r}) \sin \theta + \mathbf{k}(\mathbf{k} \cdot \mathbf{b}_{3r})(1 - \cos \theta),$$

where $\mathbf{k} = \frac{\mathbf{b}_{3r} \times \mathbf{f}_r}{\|\mathbf{b}_{3r} \times \mathbf{f}_r\|}$ and θ is the rotation angle that univocally defines $\mathbf{b}'_{3\parallel}$. Noting that the constraint $\|\mathbf{b}'_3\|^2 = 1$ is automatically verified by $\mathbf{b}'_{3\parallel}(\theta)$ for any θ , then we can further simplify (32) in terms of the only scalar variable θ as

$$\min_{\mathbf{f}_r^T \mathbf{b}'_{3\parallel}(\theta) \geq \sqrt{\|\mathbf{f}_r\|^2 - r_{xy}^2}} -\mathbf{b}_{3r}^T \mathbf{b}'_{3\parallel}(\theta). \quad (33)$$

The minimization problem (33) can be efficiently solved numerically using the bisection method shown in Algorithm 1.

In order to finally compute \mathbf{R}_d from \mathbf{b}_{3d} we suggest to employ the following formula, as done in [13]:

$$\mathbf{R}_d = \begin{bmatrix} \underbrace{(\mathbf{b}_{3d} \times \mathbf{b}_{1r}) \times \mathbf{b}_{3d}}_{\mathbf{b}_{1d}} & \underbrace{\mathbf{b}_{3d} \times \mathbf{b}_{1r}}_{\mathbf{b}_{2d}} & \mathbf{b}_{3d} \end{bmatrix}. \quad (34)$$

Finally, we note that if $\mathbf{R}_r \in \overline{\mathcal{R}(\mathbf{f}_r, \mathbf{R}_r)}$ then $\mathbf{f}_r^T \mathbf{b}_{3r} \geq \sqrt{\|\mathbf{f}_r\|^2 - r_{xy}^2}$ which, as we previously said, implies that $\mathbf{b}_{3d} = \mathbf{b}_{3r}$. Then, from (34) it results $\mathbf{R}_d = \mathbf{R}_r$, thus allowing to fulfill also the second requirement on the computation of \mathbf{R}_d , besides the minimization (15).

It is worth to notice that the described algorithm takes a negligible time to be run on a standard computer, thus allowing a real time numerical control implementation at frequencies that are way below 1 ms for each control loop, if needed by the application.

In case of different sets \mathcal{U}_{xy} and different cost functions J similar efficient approaches can be also used, which are not shown here for the sake of brevity.

V. SIMULATIONS

In this section we present the results of two numerical simulations carried out in order to test the presented controller. In particular, we simulated an LBFA of the kind described in Sec. IV.

The full-pose reference trajectories are defined in terms of the position $\mathbf{p}_r(t) = [p_{r_x}(t), p_{r_y}(t), p_{r_z}(t)]^T$ and the orientation $\mathbf{R}_r(t)$, with $t \in [0, 40]$ s. The designed trajectory has been analyzed and chosen with the purpose of being unfeasible for a standard *under-actuated* aerial robot.

In both simulations the coordinate $p_{r_z}(t)$ is kept constantly equal to 0.75 m, while $p_{r_x}(t) = A_x \sin(\bar{\omega}_x t + \delta_x)$ and $p_{r_y}(t) = A_y \sin(\bar{\omega}_y t + \delta_y)$. For the reader's visual convenience, the orientation corresponding to a rotation matrix is displayed in terms of the corresponding *roll*, *pitch*, *yaw*, with the convention $\mathbf{R}_\bullet \rightarrow \phi_\bullet, \theta_\bullet, \psi_\bullet$. However, the internal computations are all done with rotation matrices. Using this visualization, the rotational trajectory is kept constant for roll and yaw ($\phi_r(t) = \psi_r(t) = 0$ [deg]), while the pitch evolves sinusoidally: $\theta_r(t) = A_\theta \sin(\bar{\omega}_\theta t + \delta_\theta)$. Since the sinusoid in the orientation is out of phase w.r.t. the one in position, by an angle of π , it is then evident that it is unfeasible for a *collinear-thrust* platform, as the UAV would be tasked to modify its orientation while flying *backwards*.

1) *Simulation I*: In the first simulation the values given to the parameters previously defined are the following: $A_x = A_y = 0.3$ [m], $A_\theta = \frac{25\pi}{180}$ [rad], $\bar{\omega}_x = \frac{\bar{\omega}_y}{2} = 0.4$ [rad/s], $\bar{\omega}_\theta = 1$ [rad/s], $\delta_x = 0$ [rad], $\delta_y = \pi$ [rad], and $\delta_\theta = 0$ [rad].

To stress the fact that the presented controller can seamlessly work with the *under* and the *fully-actuated* platforms, we additionally modified the limit of the maximum lateral force r_{xy} exercisable by the UAV. In particular, during the simulation we started with the bound equal to zero ($r_{xy} = 0$ for $t \leq 10$ s), then we linearly increased the bound ($10 \text{ s} < t \leq 30 \text{ s}$) and finally we kept it constant ($r_{xy} = 12$ [N] for $t > 30$ s). We would like to point out that we purposefully chose wrong values for the initial velocity. This results in an increasing error in the beginning while an exponential asymptotic tracking is achieved after a few seconds. From the plots reported in Figure 5, it is straightforward to see that the change of r_{xy} affects the results, such that the trajectory tracking can be partitioned into 3 main phases: the *under-actuated phase*, the *transition phase* and the *fully-actuated phase* (i.e., with full orientation tracking).

As long as r_{xy} is exactly 0 N the system is necessarily under-actuated and so only the position reference can be tracked, while the orientation is not followed at all, due to the physical impossibility of tracking a full 6D pose: this is the case of a standard coplanar UAV. When the platform starts to gain the possibility of exerting lateral forces, then

the orientation starts to be partially tracked *in the best way*. Indeed, even if r_{xy} is not 0 anymore, the space of admissible forces might not be wide enough to contain \mathbf{f}_r . Finally, once this vector is always included in the admissible set, a value of r_{xy} large enough, the system attains a full-pose (6D) simultaneous tracking of the reference position and orientation.

2) *Simulation II*: For the second simulation, shown in the plots of Fig. 6, we propose a different trajectory. The lateral bound is kept this time constant at $r_{xy} = 12$ [N]. While the reference orientation is the same of the previous case, $\bar{\omega}_x$ and $\bar{\omega}_y$ are varying with time, starting from a high value ($\bar{\omega}_x = 20$ [rad/s], $\bar{\omega}_y = 40$ [rad/s]) to then finally converge to zero. The results for p_{r_x} and for p_{r_y} are then 2 swinging sinusoidal signals which slowly converge to constant ones. Even the amplitude for the sinusoidal positions are larger, being this time $A_x = A_y = 1.2$ [m].

The goal is to show that, even in presence of a hard demanding reference trajectory, the controller ensures the convergence of the position error to zero, after an initial transient due to the fact that the platform starts with zero conditions of position, velocity and acceleration while the reference signal is quickly changing. As far as the orientation is concerned, our strategy guarantees that the *best feasible* one will be followed. As the frequency of the sinusoidal positions is decreasing, then \mathbf{R}_d converges to \mathbf{R}_r , and so does \mathbf{R} .

VI. CONCLUSIONS

In this paper we introduced the new class of Laterally-Bounded Fully-Actuated (LBFA) aerial vehicles. This class is general enough to encompass a large variety of recently conceived aerial vehicles having the possibility to actuate the thrust in a direction other than the principal one. Common underactuated platforms are included in this class as a degenerate (but fully admissible) case.

For this class of vehicles we proposed a geometric controller in SE(3) that is able to let it track a full-pose (6D) trajectory. The controller adapts seamlessly to the case the trajectory is (or becomes) not feasible or that the platform is (or becomes) underactuated. Being defined in SE(3) the controller is not prone to the singularities of local chart orientation representations.

In future we plan to test the controller with a real aerial LBFA platform that we are currently developing. Furthermore it will be interesting to study adaptive and robust techniques to deal with parameter uncertainties and loss of some of the actuators.

REFERENCES

- [1] T. Tomić, K. Schmid, P. Lutz, A. Dömel, M. Kassecker, E. Mair, I. L. Grixa, F. Ruess, M. Suppa, and D. Burschka, "Toward a fully autonomous uav: Research platform for indoor and outdoor urban search and rescue," *Robotics & Automation Magazine, IEEE*, vol. 19, no. 3, pp. 46–56, 2012.
- [2] N. Kenzo, "Prospect and recent research and development for civil use autonomous unmanned aircraft as uav and mav [j]," *Journal of System Design and Dynamics*, vol. 1, no. 2, pp. 120–128, 2007.
- [3] S. Waharte and N. Trigoni, "Supporting search and rescue operations with uavs," in *Emerging Security Technologies (EST), 2010 International Conference on*. IEEE, 2010, pp. 142–147.

- [4] ARCAS, "EU Collab. Project ICT-287617," www.arcas-project.eu, 2011-2015.
- [5] SHERPA, "EU Integrated Project IP 600958," www.sherpa-project.eu.
- [6] AeRoArms, "EU Collab. Project ICT-644271," www.aeroarms-project.eu, 2015-2019.
- [7] A. Albers, S. Trautmann, T. Howard, T. A. Nguyen, M. Frietsch, and C. Sauter, "Semi-autonomous flying robot for physical interaction with environment," in *Robotics Automation and Mechatronics (RAM), 2010 IEEE Conference on*. IEEE, 2010, pp. 441–446.
- [8] I. Maza, K. Kondak, M. Bernard, and A. Ollero, "Multi-uav cooperation and control for load transportation and deployment," *Journal of Intelligent and Robotic Systems*, vol. 57, no. 1-4, pp. 417–449, 2010.
- [9] R. Voyles and G. Jiang, "Hexrotor UAV platform enabling dextrous interaction with structures – preliminary work," in *2012 IEEE Int. Symp. on Safety, Security and Rescue Robotics*, College Station, TX, Nov. 2012, pp. 1–7.
- [10] H. Romero, S. Salazar, A. Sanchez, and R. Lozano, "A new uav configuration having eight rotors: Dynamical model and real-time control," in *Decision and Control, 2007 46th IEEE Conference on*. IEEE, 2007, pp. 6418–6423.
- [11] M. Ryll, H. H. Bühlhoff, and P. Robuffo Giordano, "A novel over-actuated quadrotor unmanned aerial vehicle: modeling, control, and experimental validation," *IEEE Trans. on Control Systems Technology*, vol. 23, no. 2, pp. 540–556, 2015.
- [12] S. Rajappa, M. Ryll, H. H. Bühlhoff, and A. Franchi, "Modeling, control and design optimization for a fully-actuated hexarotor aerial vehicle with tilted propellers," in *2015 IEEE Int. Conf. on Robotics and Automation*, Seattle, WA, May 2015, pp. 4006–4013.
- [13] T. Lee, M. Leoky, and N. H. McClamroch, "Geometric tracking control of a quadrotor UAV on SE(3)," in *49th IEEE Conf. on Decision and Control*, Atlanta, GA, Dec. 2010, pp. 5420–5425.
- [14] V. Mistler, A. Benallegue, and N. K. M'Sirdi, "Exact linearization and noninteracting control of a 4 rotors helicopter via dynamic feedback," in *10th IEEE Int. Symp. on Robots and Human Interactive Communications*, Bordeaux, Paris, France, Sep. 2001, pp. 586–593.
- [15] S. Bouabdallah and R. Siegwart, "Backstepping and sliding-mode techniques applied to an indoor micro quadrotor," in *2005 IEEE Int. Conf. on Robotics and Automation*, May 2005, pp. 2247–2252.
- [16] H. Romero, S. Salazar, A. Sanchez, and R. Lozano, "A new UAV configuration having eight rotors: dynamical model and real-time control," in *46th IEEE Conf. on Decision and Control*, New Orleans, LA, Dec. 2007, pp. 6418–6423.
- [17] D. Mellinger and V. Kumar, "Minimum snap trajectory generation and control for quadrotors," in *2011 IEEE Int. Conf. on Robotics and Automation*, Shanghai, China, May. 2011, pp. 2520–2525.
- [18] M.-D. Hua, T. Hamel, P. Morin, and C. Samson, "Control of VTOL vehicles with thrust-tilting augmentation," *Automatica*, vol. 52, pp. 1–7, 2015.
- [19] S. Prothin and J.-M. Moschetta, "A vectoring thrust coaxial rotor for micro air vehicle: Modeling, design and analysis," in *ERCOTAC international symposium 'Unsteady separation in fluid-structure'*, Mykonos, Greece, June. 2013.

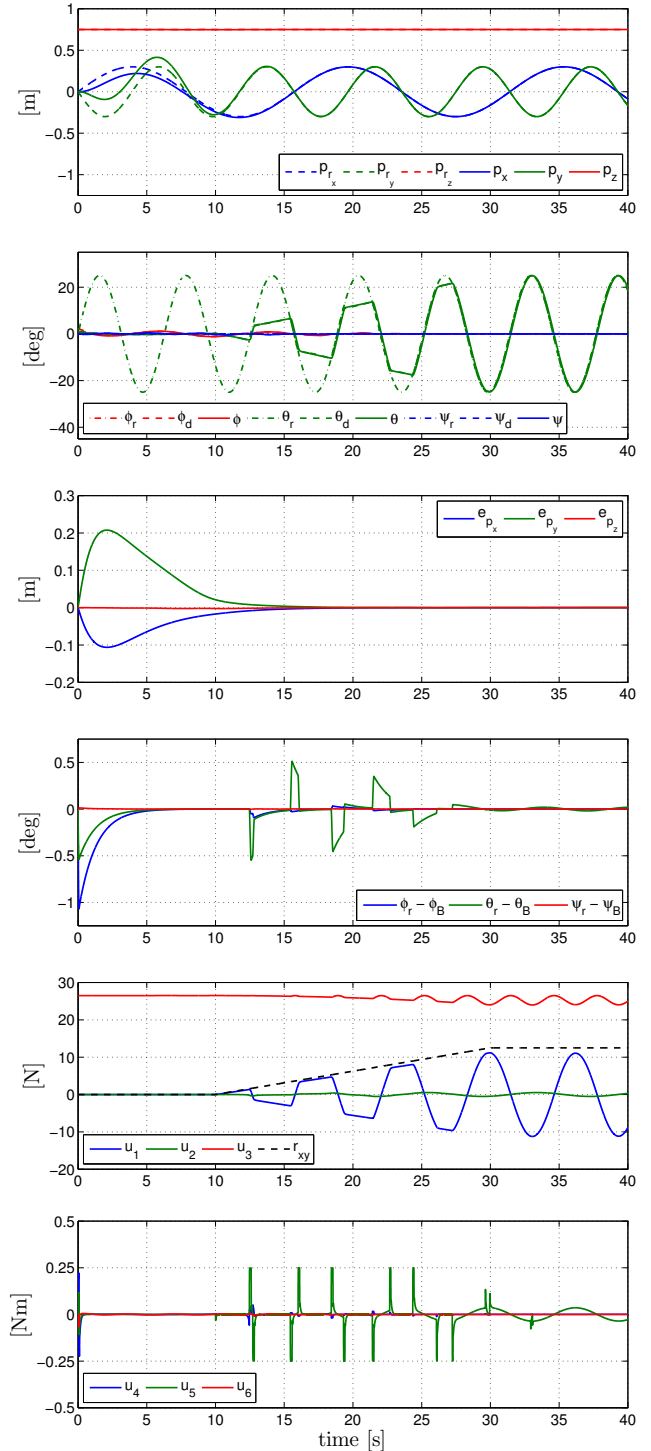


Fig. 5. Simulation 1: Tracking of the complete 6D pose with a reference trajectory with p_{rx} , p_{ry} , θ_r sinusoidally-shaped with different phases. What is not feasible for a standard underactuated quadrotor becomes possible for a LBFA UAV, once r_{rx} is increasing. The proposed controller works seamlessly in any r_{xy} condition. All the symbols are defined in the paper.

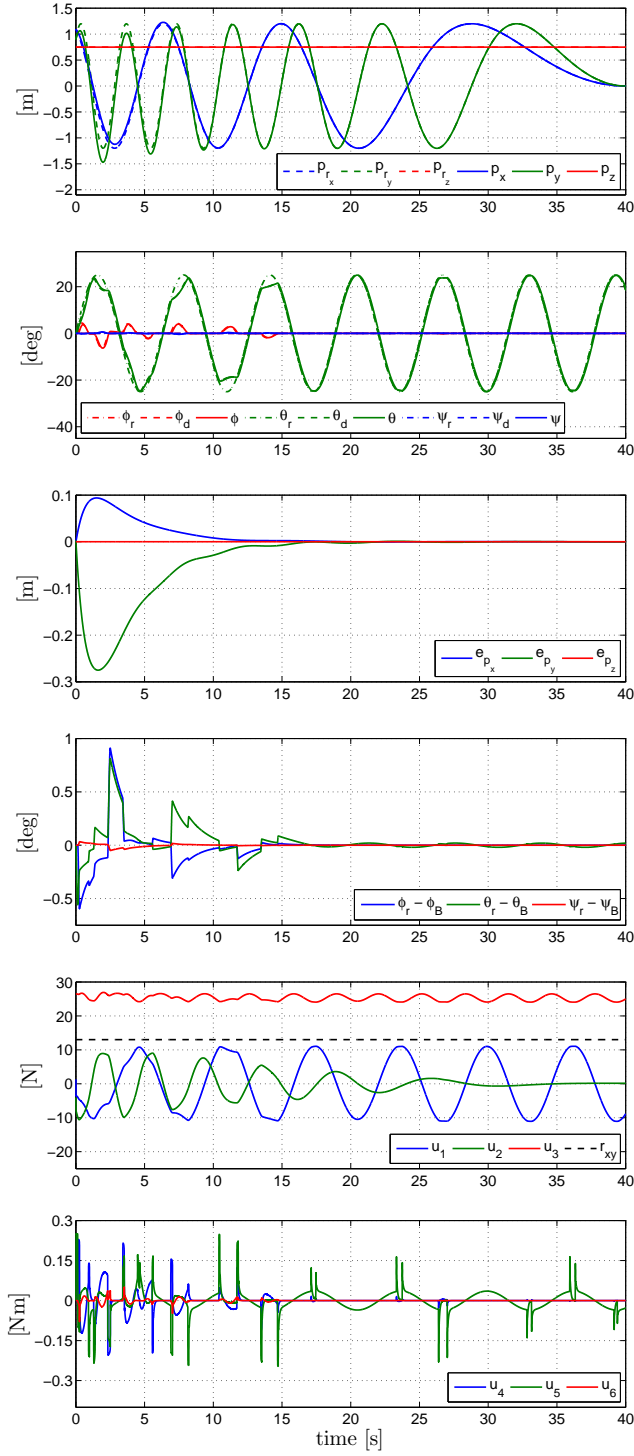


Fig. 6. Simulation 2: Tracking of the complete 6D pose with a reference trajectory with p_{rx} , p_{ry} , θ_r sinusoidally-shaped with different phases and varying angular frequencies $\omega_{\bullet}(t)$. During the simulation the value of each frequency starts from a strong value to then decreases to zero. The value of of the lateral bound r_{xy} is kept constant.